Amine-functionalized CNTs@mSiO$_2$ with short radical mesochannels for fast and efficient CO$_2$ capture

Liju Bai[a], Xiaotong Jiang[a], Yimin Deng[a], Shuai Wang[a], Helei Liu[a*]

[a] Joint International Research Laboratory of Carbon Neutrality System and Engineering Management, Beijing Laboratory for System Engineering of Carbon Neutrality, School of Chemistry and Chemical Engineering, Beijing Institute of Technology, Beijing, 102488, China

*Authors for correspondence: Dr. Helei Liu, Email: lhl0925@hotmail.com, hl_liu@bit.edu.cn

Analytical tools

Scanning Electron Microscopy (SEM) images were obtained on a ZEISS GeminiSEM 360 high-resolution SEM with an accelerating voltage of 2.0 kV. The samples were dispersed on conductive carbon tape, mounted on stubs. X-ray photoelectron spectroscopy (XPS) was performed on an AXIS ULTRA DLD XPS system (Shimadzu Corp.) to characterize the NH$_2$-modified mesoporous silica. Transmission electron microscopy (TEM) images were acquired on JEM-2100F transmission electron microscope with an accelerating voltage of 200 kV equipped with a post-column Gatan imaging filter (GIF-Tridium). Fourier-transform infrared (FT-IR) were performed on the Thermo IS5. Spectra were collected on the neat samples and at room temperature (around 25°C). Spectra are plotted in transmittance (%) against the wavenumbers (cm^{-1}). The Brunauer-Emmett-Teller (BET) method was used to calculate specific surface areas using adsorption data (BELSORP MAX II). The Barrett-Joyner-Halenda (BJH) model was used to calculate pore size distributions derived from adsorption branches. The static adsorption capacity of CO$_2$ at different temperatures from 0 to 1bar was determined by isothermal adsorption model. The intelligent mass analyzer IGA-100 was used to determine the CO$_2$ adsorption kinetics, and the time and amount of CO$_2$ adsorption were plotted.

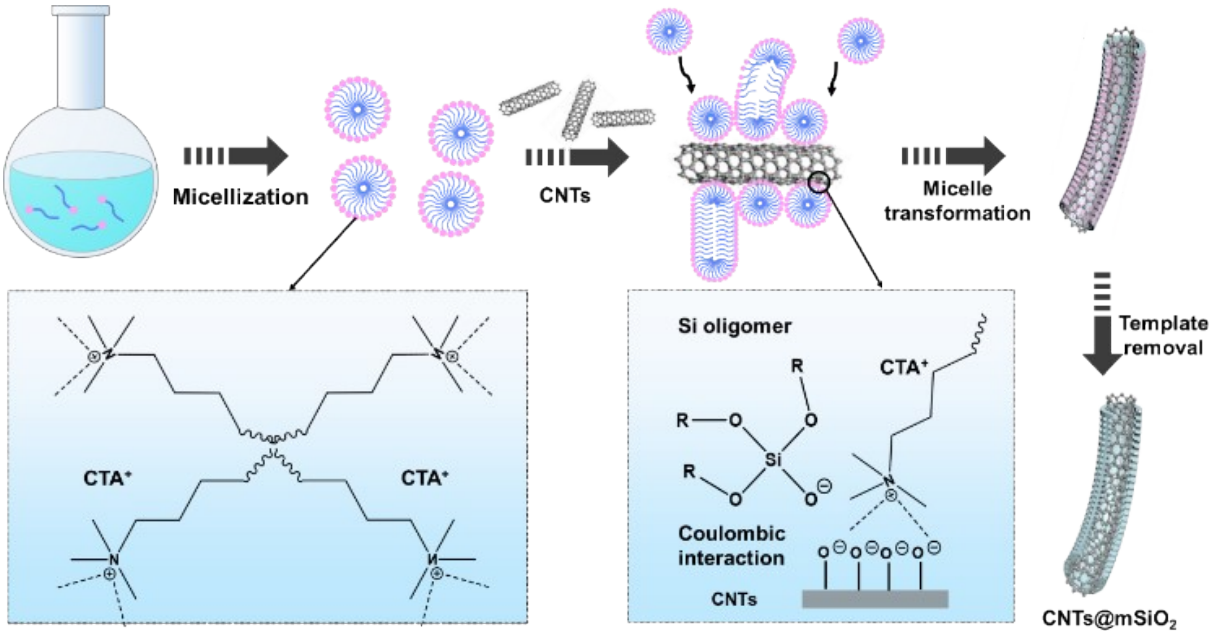

Figure S1 Synthesis strategy for high specific surface area CNTs@mSiO_2. Illustration of self-assembly of CTAB micelles and TEOS hydrolyzed oligomers onto the surface of CNTs using Van Der Waals attraction. Removal of CTAB exposes the short mesoporous network.

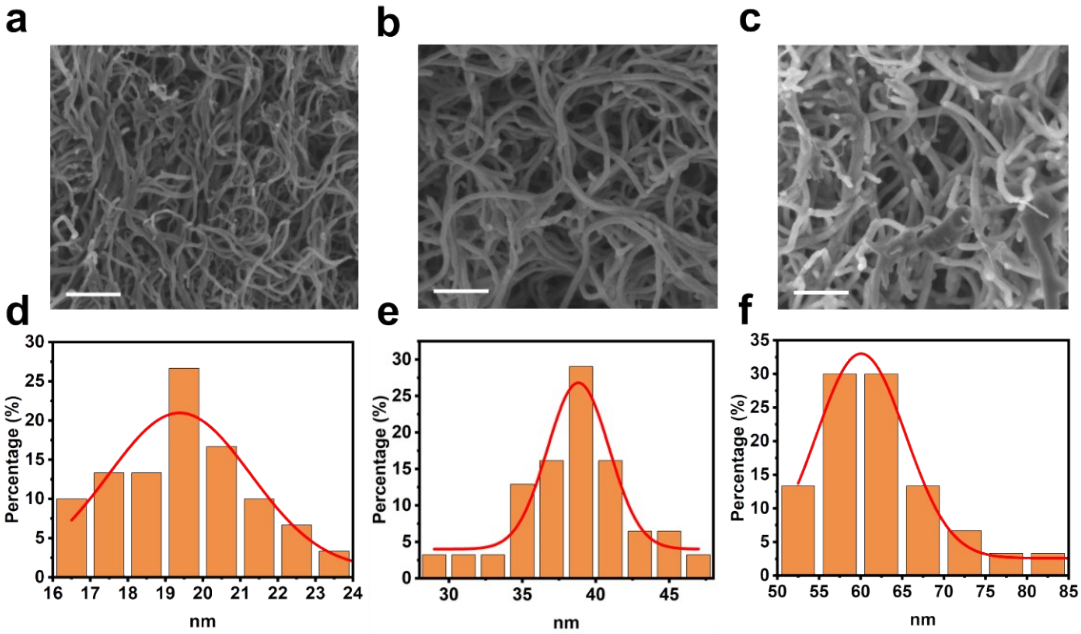

Figure S2 SEM images of (a) CNTs@0.6SiO_2, (b) CNTs@1.2SiO_2 and (c) CNTs@1.6SiO_2. Scale bars are 200 nm. Diameter distribution histogram of (d) CNTs@0.6SiO_2, (e) CNTs@1.2SiO_2 and (f) CNTs@1.6SiO_2.

Table S2 The pore structure of different CNTs@mSiO_2

CNT	BET	Pore size	Pore volume	Diameter	Pore length

	($m^2 g^{-1}$)	(nm)	($cm^3 g^{-1}$)	(nm)	(nm)
CNTs@0.6SiO_2	609.9	1.2	0.691	~20	~4
CNTs@1.2SiO_2	950.1	2.4	0.774	~40	~12
CNTs@1.8SiO_2	1036.1	2.2	0.639	~60	~22

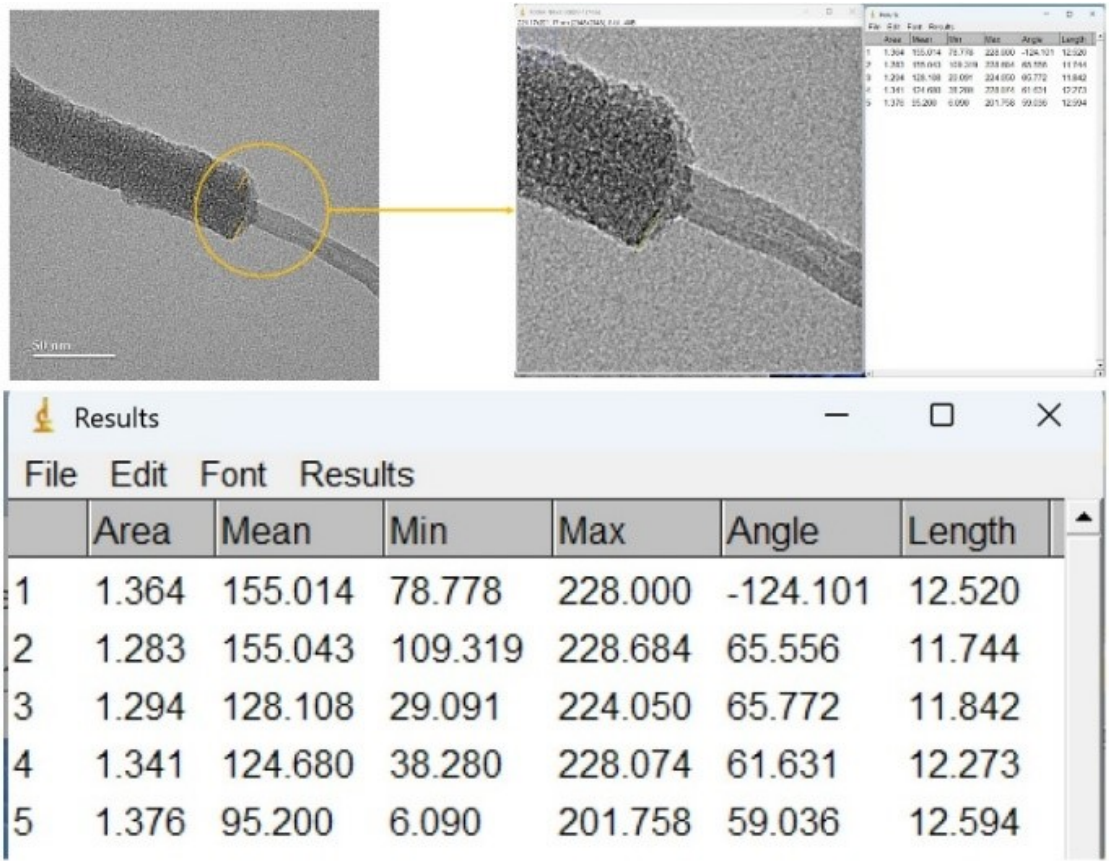

Figure S3 Use Image-J to measure the length of the chanel.

Amino-functionalization methods

Table S2 Structural and physical properties of amines used in the vapour phase impregnation.

Amine	Molecular wight (g/mol)	Boiling point (°C)	Structure	Diameter (Å)
Piperazine	86.1	146	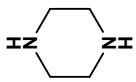	7.375*4.495*4.019

Ethylenediamine	60.1	116	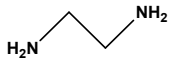	7.004*6.401*4.818
1,3-Propanediamine	89.14	155		7.259*5.324*4.828

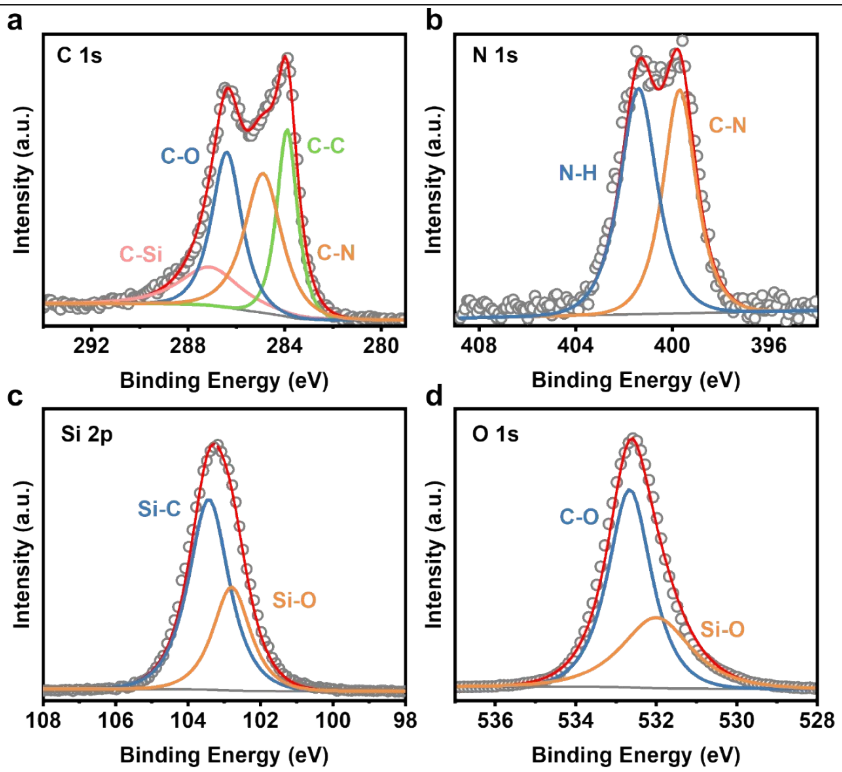

Figure S4 Fine C1s, N1s, Si2p and O1s XPS spectra of CNTs@mSiO_2-ED

CO_2 capture performance

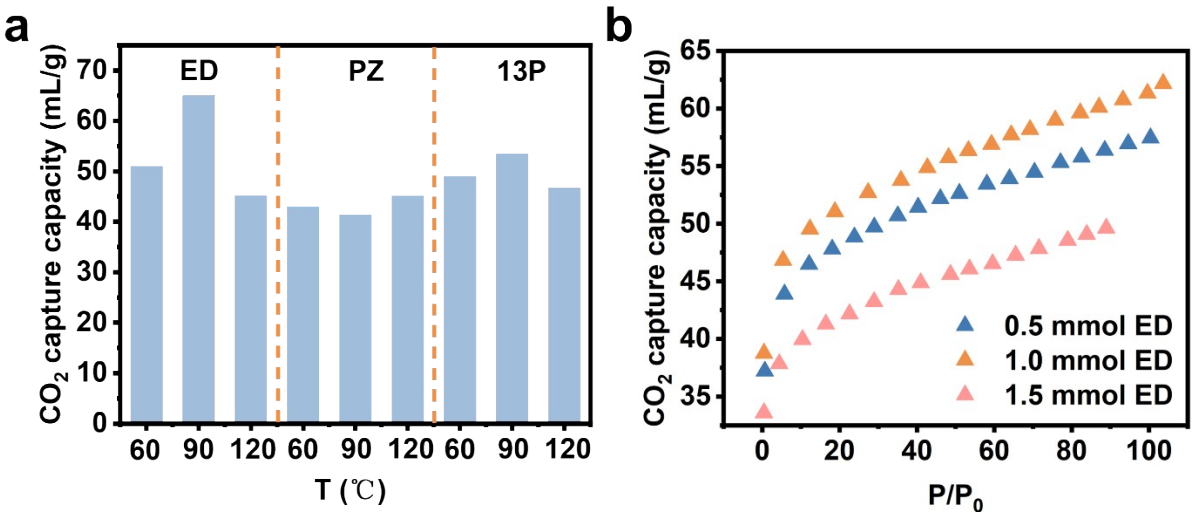

Figure S5 CO_2 capture capacity of (a) different amine types and (b) grafting amount of amines

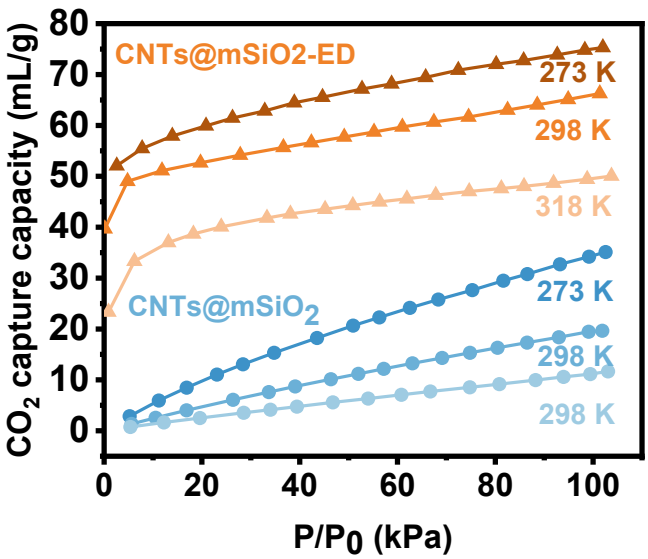

Figure S6 The CO_2 capture capacity of CNTs@mSiO$_2$-ED and CNTs@mSiO$_2$ at different temperature.

CO_2/N_2 selective adsorption

To conclude, the selectivity factors, $S_{1,2}$ (where 1=CO_2 and 2=N_2), were calculated using Equation S(1), described by Cueto-Diaz et al.

$$S_{i,j} = \frac{x_i/y_i}{x_j/y_j} = \frac{P_j^0}{P_i^0} \qquad S(1)$$

The theoretical maximum value $S_{1,2}$ is given when the gas consists of pure nitrogen (yCO_2=0) and the theoretical minimum one for the case that the gas is pure CO_2 (yCO_2=1).

Reaction heat

The isotherm heat is a critical thermodynamic parameter for evaluating the interaction between adsorbent and the adsorbate, which reveals the strength of the interaction between the CO_2 molecule and the adsorption site of the amine group. The isotherm heat (Q) can be calculated by the Clausius-Clapeyron equation with adsorption data at different temperatures[1]:

$$Q = R \times T_1 \times T_2 \times \ln\left(\frac{P_2}{P_1}\right)/(T_2 - T_1) \qquad S(2)$$

Where Q (J mol^{-1}) is the absorption heat, R is the gas constant 8.314 J mol^{-1} K^{-1}. T_1 and T_2 (K) are the measured adsorption temperatures. P_1/P_2 (Pa), the adsorption pressure corresponding to the same adsorption amount on the measured isotherms of the sample at the above two

adsorption temperatures.

Table S3 Adsorption and dynamic properties of selected CO_2 capture adsorbents.

Material	t_{50} (min)	CO_2 capture capacity (mmol/g)	t_{50} rate (mmol/g/min)	Ref
Aminosilica	2.02	26.43	13.08	[2]
Amino-rich mesoporous silica	3.50	25.98	7.41	[3]
AmSic	37.53	21.80	0.58	[4]
45%PEI@SBA-15	10.05	51.05	5.08	[5]
55%PEI@MCM-41	5.56	24.53	4.41	[5]
50%PEI/SBA-15	86.38	32.57	0.38	[6]
50%TEPA/SBA-15	90.99	50.40	0.56	[6]
PEI silica	3.05	25.33	8.31	
MCM-41-PEI40	1.02	33.69	33.20	[7]
MCM-41-PEI60	1.61	46.48	28.81	[7]
A-BK-TEPA-50	6.08	85.05	14.00	[8]
5PZ/silica	1.17	25.74	21.91	[9]
60EG/S	2.50	29.48	11.80	[10]
SBA-D-4.6	0.43	16.02	37.07	[11]
OHNS-AAMS@298 K	321.70	28.81	0.02	[12]
PM01	13.54	16.62	0.09	[13]
Al-MCM-41-0.3	0.83	27.33	1.23	[14]
HMS-TEPA70%	7.97	130.59	32.84	[15]
CNTs@mSiO_2-ED	1.93	68.10	14.22	This work

Dynamic properties

In the present work, a pseudo-first-order, pseudo-second-order, and Elovich equation were used to investigated the kinetic properties of CO_2 adsorption on CNTs@mSiO_2-1ED[16]. Information on the models is displayed ad follows:

(1) Pseudo-first-order

$$q_t = q_e[1 - exp(-k_1 t)] \qquad S(3)$$

(2) Pseudo-second-order

$$q_t = k_2 q_e^2 t/(1 + k_2 q_e t) \qquad S(4)$$

(3) Elovich

$$q_t = \frac{1}{b} ln(ab) + \frac{1}{b} lnt \qquad S(5)$$

Where t is adsorption time. k_1 and k_2 are adsorption rate constants in the pseudo-first-order and pseudo-second-order. Q_t and q_e stand for the CO_2 adsorption capacity at a certain moment and the saturated adsorption capacity, respectively. a and b represent the initial adsorption rate constant and the desorption rate constant, respectively.

(4) Internal diffusion model

$$q_t = kt^{0.5} + C \qquad S(6)$$

Table S4 Molecular dynamics simulation.

	C_0	k_1	C_1	R^2	k_2	C_2	R^2	k_3	C_3	R^2
CNTs@mSiO$_2$-1ED	62	22.65	-2.31	0.99	4.14	31.73	0.98	0.50	58.30	0.90
SBA-15-1ED	38	15.11	-4.75	0.96	3.12	18.82	0.99	0.23	39.92	0.98

N content after amine functionalization

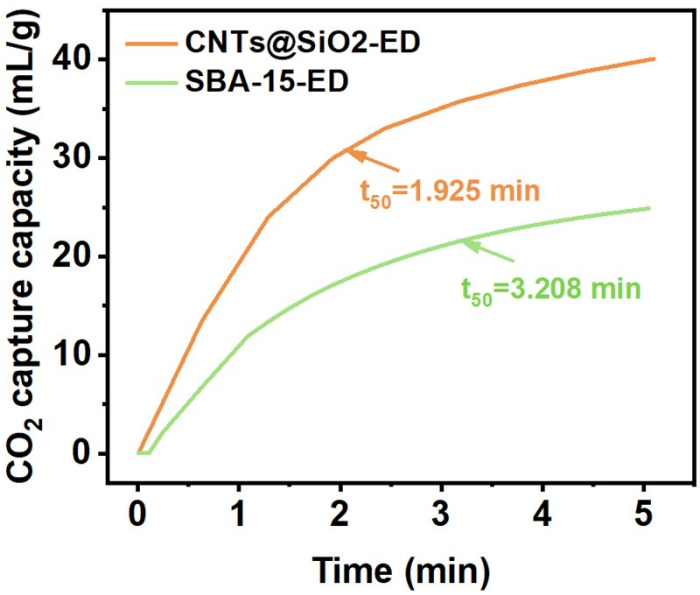

Figure S7 The adsorption kinetics curve of CNTs@SiO_2-ED and SBA-15-ED

Comparison with literature data

Different pore lengths CNTs@mSiO_2 Material characterizationComputational methods

In this study, the cell model of SiO_2 was obtained from The Cambridge Crystallographic Data Center (CCDC, ID2259819)[17]. The high-precision ab initio density-functional theory method is adopted at the electron scale, and the CASTEP calculation module in Material Studio was conducted to select the GGA local exchange correlation general function for optimization, and the optimization parameters are set as follows: cut-off energy cut off 500.0 eV, Brillouin zone k-point 1×1×1, and the total energy of each atom self-consistency converges to within 1×10^{-5} eV to obtain the lowest energy of the system. 1, and the total electron self-consistent energy of each atom converges to within 1×10^{-5} eV to obtain the lowest energy of the system. CASTEP handles the calculation of the complex system, and the lowest energy structure of the system is obtained by the DFT calculation based on the Kohn-Sham equation.

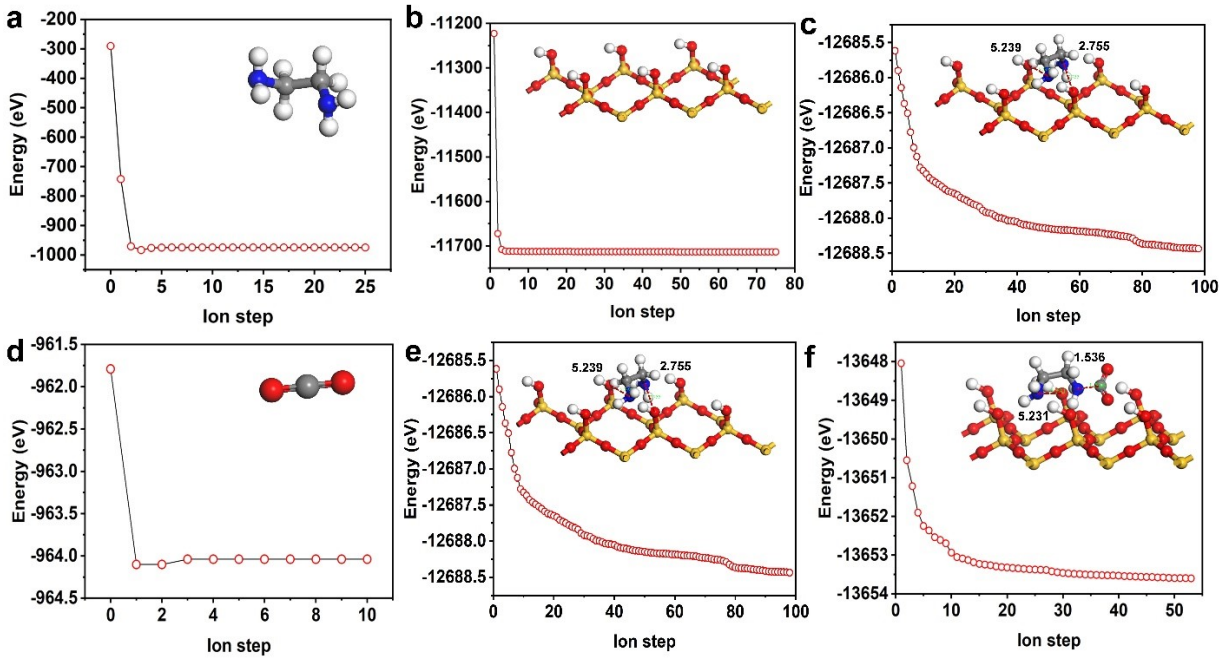

Figure S8 Energy convergence for geometric optimization and structures of (a) Ethylenediamine (b, e) the pore wall of CNTs@mSiO_2 (c) SiO_2-ED (d) CO_2 and (f) CNTs@mSiO_2-ED-CO_2 after geometric optimization of DFT, respectively.

References

1. X. An, K. Zhao, W. Pang, W. Zhang, L. Wang, T. Guo and D. Fu, *Chemical Engineering Journal*, 2022, **431**.

2. S. Ahsan, A. Ayub, D. Meeroff and M. Jahandar Lashaki, *Chemical Engineering Journal*, 2022, **437**.
3. B. Zhang, X. Liu, H. Wang, K. Li, T. Tatsumi and J. Wang, *Materials Letters*, 2022, **321**.
4. T. Kataoka, Y. Orita and Y. Shimoyama, *Chemical Engineering Journal*, 2024, **482**.
5. Y. Zhang, S. Zhao, L. Li, J. Feng, W. Qiu, Z. Wei, X. Li, Z. Huang and H. Lin, *Gas Science and Engineering*, 2024, **123**, 205251.
6. Y. Miao, Z. He, X. Zhu, D. Izikowitz and J. Li, *Chemical Engineering Journal*, 2021, **426**.
7. X. Jia, P. Yang, Y. Fan and C. Wang, *Separation and Purification Technology*, 2024, **328**.
8. Y. Yuan, J. Wei, L. Geng, D. Mei and L. Liao, *RSC Advances*, 2020, **10**, 34187-34196.
9. L. Liu, Q. Wang, Y.-H. Cho, H.-H. Park and C.-H. Lee, *Chemical Engineering Research and Design*, 2023, **199**, 74-86.
10. A. Z. Sheshkovas, J. V. Veselovskaya, V. A. Rogov and D. V. Kozlov, *Microporous and Mesoporous Materials*, 2022, **341**.
11. F. Bai, X. Liu, S. Sani, Y. Liu, W. Guo and C. Sun, *Separation and Purification Technology*, 2022, **299**.
12. K. S. K. Reddy, A. M. Varghese, A. E. Ogungbenro and G. N. Karanikolos, *ACS Applied Engineering Materials*, 2023, **1**, 720-733.
13. A. A. Al-Absi, M. Mohamedali, A. Domin, A. M. Benneker and N. Mahinpey, *Chemical Engineering Journal*, 2022, **447**.
14. M. Jahandar Lashaki, H. Ziaei-Azad and A. Sayari, *Chemical Engineering Journal*, 2022, **450**.
15. P. Zhao, G. Zhang, Y. Xu and Y. Lv, *Journal of CO2 Utilization*, 2019, **34**, 543-557.
16. M. Liao, S. Long, P. Zou, K.-Y. Zhang, H.-C. Liang, K. Jiang, D. Xie and F.-M. Yang, *Energy & Fuels*, 2023, **37**, 15867-15878.
17. I. Grosskreuz and B. Marler, *Zeitschrift für Kristallographie - New Crystal Structures*, 2023, **238**, 655-657.